One year of 222Rn concentration in the atmospheric surface layer

S. Galmarini

▶ **To cite this version:**

S. Galmarini. One year of 222Rn concentration in the atmospheric surface layer. Atmospheric Chemistry and Physics Discussions, 2005, 5 (6), pp.12895-12937. hal-00301997

HAL Id: hal-00301997
https://hal.science/hal-00301997

Submitted on 18 Jun 2008

HAL is a multi-disciplinary open access archive for the deposit and dissemination of scientific research documents, whether they are published or not. The documents may come from teaching and research institutions in France or abroad, or from public or private research centers.

L'archive ouverte pluridisciplinaire **HAL**, est destinée au dépôt et à la diffusion de documents scientifiques de niveau recherche, publiés ou non, émanant des établissements d'enseignement et de recherche français ou étrangers, des laboratoires publics ou privés.

Atmos. Chem. Phys. Discuss., 5, 12895–12937, 2005
www.atmos-chem-phys.org/acpd/5/12895/
SRef-ID: 1680-7375/acpd/2005-5-12895
European Geosciences Union

Atmospheric Chemistry and Physics Discussions

One year of ^{222}Rn concentration in the atmospheric surface layer

S. Galmarini

Institute for Environment and Sustainability, Joint Research Center, 21020 Ispra, Italy

Received: 22 July 2005 – Accepted: 6 September 2005 – Published: 19 December 2005

Correspondence to: S. Galmarini (stefano.galmarini@jrc.it)

© 2005 Author(s). This work is licensed under a Creative Commons License.

Abstract

A one-year time series of ^{222}Rn measured in a rural area in the North of Italy in 1997 is analyzed. The scope of the investigation is to better understand the behavior of this common atmospheric tracer in relation to the meteorological conditions at the release site. Wavelet analysis is used as one of the investigation tools of the time series. The measurements and scalograms of ^{222}Rn are compared to those of wind-speed, pressure, relative humidity, temperature and NO_x. The use of wavelet analysis allows the identification of the various scales controlling the influence of the meteorological variables on ^{222}Rn dispersion in the surface layer that are not visible through classical Fourier analysis or direct time series inspection. The analysis of the time series has identified specific periods during which the usual diurnal variation of radon is superimposed to a linear growth thus indicating the build up of concentration at the measurement level. From these specific cases an estimate of the surface flux of ^{222}Rn is made. By means of a simple model these special cases are reproduced.

1. Introduction

Radon emission from the ground has long been studied over the last decades from several view points. As radioactive product of the uranium chain, it is abundant all over the Earth crust and constantly emitted from the ground. The noble gas chemical form makes radon invulnerable to wet deposition or chemical reaction thus allowing an undisturbed transport in the atmosphere as well as closed environments such as households or working places. Radioactive decay is the only removal process. We will not discuss here the potential health threat of radon as it has been debated over the years and it is still being debated intensively. Apart from this aspect, which is in any case very relevant, radon represents a very interesting natural tracer for a number of atmospheric research studies. It has long been studied in the atmospheric boundary layer (ABL) as constantly emitted from the surface (e.g. Israël et al., 1966; Ikebe and

ACPD

5, 12895–12937, 2005

Shimo, 1972; Beck et al., 1979; Vinod Kumar et al., 1999; Sesana et al., 2003, 2005; Pearson and Moses, 1966; Marcazan et al., 1993, 1997; Kataoka et al., 2001, 2003), to characterize the turbulent diffusion properties of the lower atmospheric levels, and since some of its radio nuclides have decay timescales comparable to that of turbulent transport in the ABL (e.g. Beran and Assaf, 1970; Druilhet and Fontan, 1973; Kristensen et al., 1997). Similarly intensive research has been conducted at global scale where radon is used for global atmospheric chemistry models evaluation (e.g. Dentener et al., 1999), as well as for the estimate of the fluxes of the atmospheric constituents or pollutants. For a detailed review on the radon studies and sampling techniques in atmospheric science refer to Zahorowski et al. (2004).

In the present study a one-year time series of radon-222 measured in the atmospheric surface layer (ASL) is analyzed. The data were collected in 1997 on the premises of the European Commission Joint Research Center within a collaboration project between the latter and the Faculty of Physics of the University of Milan (Facchini et al., 1999). Although the time series is obtained as 1-h average concentration at a fixed location and height, its analysis highlights a series of features that where not investigated before.

In the first part of this study we will focus on the relationship between the time evolution of radon and that of the meteorological parameters. Although the influence of the latter on radon emission and time evolution is rather well known, in this context we will focus on the relationship between the scales of occurrence of the various meteorological events and those of radon dispersion in the ASL. Towards this purpose, a time series analysis is conducted by means of wavelets (Farge, 2000; Farge and Schneider, 2002). It is a technique for the determination of localized (in time or in space) power spectra which adapts very well to the analysis of signals with a strong time or space variability. Several studies in the past have clearly demonstrated the capacity of this technique to highlight fundamental features of a signal that would not be otherwise distinguished by classical time series analysis or Fourier transformation (e.g. Druhilet et al., 1994; Gao et al., 1993; Galmarini and Attié, 1999; Attié and Durand, 2003;

Salmond, 2005). In the second part of the paper some specific features identified in the time series will be analyzed and modeled. In general the following research issues are addressed:

- Analysis of the one-year time series and investigation of the monthly variability of radon concentration;
- Dependence of hourly concentration at the surface on meteorological parameters;
- Comparison between radon concentration and the one of other atmospheric tracers;
- Analysis of specific peculiarities in the radon time series and provision of explanations, including the determination of the surface flux from mean concentration values.

2. Description of the data

The data analyzed consist of one year of continuous measurements with one hour resolution of the variables of Table 1. The sampling location is within the Joint Research Center (JRC) premises and corresponds to an official EMEP site (station IT04 (45°48′ N; 8°38′ E) – 209 m a.s.l.). The JRC is located in the Po Valley at the foothills of the western Alps on the eastern shore of Lago Maggiore. At the station, variables 1–7 are regularly measured together with a variety of other chemical compounds (Leyendecker, 1998). The radon measurements were conducted specifically over the period December 1996–January 1998, and are not part of the ordinary station instrumentation. The radon sampling was performed by means of a monitor developed by the University of Milan and described in detail in Facchini et al. (1999) and Sesana et al. (2003). The instrument detects directly ^{222}Rn that is therefore not inferred from the analysis of its daughters as in other cases (Marcazzan et al., 1993 and 1997). Air was sampled at 3 m from the surface. The time series from 1 January to 31 December 1997

ACPD
5, 12895–12937, 2005

is complete, except for 4 days in July (22–24 July 1997, 28–29 July 1997), 5 days in November (13–18 November 1997) during which no radon concentrations were collected. Occasionally measurements were not collected over time intervals of one hour. In this case the values where interpolated from the preceding and succeeding measurements.

Figure 1 shows the time evolution of the variables of Table 1 including a 24-h running mean thus providing a clear characterization of the sampling location for the year analyzed. The most important aspects are:

- The absence of strong winds exception for katabatic flows connected to the vicinity of the Alps and local breezes due to the vicinity of the lake basin.
- The temperature evolution through out the year is typical of a mid latitude location with cold winters and fairly warm summers.
- Relative humidity is fairly high through out the year due to the presence of the lake basin and the stagnation of air masses within the Po Valley.
- Very small precipitation (a particularly dry year for the region) mainly characterized by short periods of relatively intense rain.
- Nitrogen oxides are fairly abundant due to the rural character of the area but also the relative vicinity of industrial areas and intense traffic roads.
- Radon's concentration is also fairly high ranging from a minimum value of few Bqm^{-3} in May to a maximum 50 Bqm^{-3} in December.

The correlation between radon concentration and the other variables is also given in Table 1. All correlations are consistent with the expectations. Namely, negative correlation with wind speed and precipitation responsible for reducing the concentration in the boundary layer and its emission at the surface respectively; negative correlation with temperature which has an opposite diurnal cycle compared to radon. High positive

correlation with relative humidity is found, which on the contrary has a similar diurnal cycle; and also a fairly large positive correlation with NO_x. The correlation with atmospheric pressure is positive in contrast with what found by other studies (e.g. Moses et al., 1973).

3. Wavelet analysis of radon monthly evolution

We start by analyzing the Fourier spectrum of the one-year time series of the variables of Table 1 in order to first identify globally the dominant scales. Figure 2a shows the power spectrum of the meteorological variables and NO_x and Fig. 2b the spectrum of radon. As pointed out by Torrence and Compo (1998) a power spectrum analysis of geophysical data requires the definition of a null-hypothesis to be used as term of comparison of the actual signal spectrum and for the identification of significant features within it. The figures also display the red noise spectrum obtained from the parameterization by Gilman et al. (1963) and the 95% confidence spectrum. The first is obtained from:

$$P_k = \frac{1 - \alpha^2}{1 + \alpha^2 - 2\alpha \cos\left(\frac{2\pi k}{N}\right)} \quad (1)$$

for k=1, ... N/2, where N is the number of samples, α is given by:

$$\alpha = \frac{\alpha_1 + \sqrt{\alpha_2}}{2} \quad (2)$$

In Eq. (2), α_1 and α_2 are respectively the lag-1 and lag-2 autocorrelation coefficients of the variables analyzed. Figures 2a and b also show the spectrum obtained by a running average of the original one with a pace of 12 h.

As far as the meteorological variables and NO_x are concerned we can notice the following:

ACPD
5, 12895–12937, 2005

- Wind speed: The spectrum is above the red noise one up to a period of 30–40 h, and is significant below the 12 h scale. Energy peaks can be noticed at 8 and 12 h. This clearly indicates the presence of periodic processes like lake breeze that have a diurnal or semi diurnal periodicity.

- Temperature, relative humidity and NO_x: The spectra of these three variables are comparable as they are all atmospheric tracers transported and diffused in a similar way. They all show the presence of significant peaks at 24, 12, 8, 6 and 4 h. In the case of temperature peaks are also visible at 3 h time scale.

- Pressure: even in the case of pressure we can notice the presence of peaks at the diurnal and semi diurnal scale though the associated variance is much smaller compared to the other variables.

- Precipitation: No clear structure is present in the case of precipitation which shows a significant signal only at periods smaller than 10 h, due to the scarce and short precipitation events.

The similarities between the radon spectrum and the one of the other tracers can be seen by analyzing Fig. 2b. In general, up to a scale of 50 h the radon spectrum lays above the red noise power spectrum and it is above the 95% confidence spectrum up to a scale of 20 h. Within this range of scales one can clearly distinguish the presence of six energy peaks positioned at 24.063 h, 11.98 h, 7.99 h, 5.9 h, 4.79 h. All the peaks refer to the daily evolution of radon concentration which is governed by the daily evolution of the boundary layer depth and the constant emission from the surface. The shortest time scales are however indicating the occurrence of processes affecting the concentration and that produce a variance at smaller scales than the half day or 24 h cycle. The result presented in Fig. 2b is not completely surprising as the mechanism of radon emission and dispersion in the boundary layer are known and given the spectrum of the other variables described above. However, it represents just a global analysis which does not provide any insight on the actual concentration time

series. Therefore, it is interesting to verify whether the peaks at periods smaller than 24 h are a constituting feature of the dataset or associated to specific processes and time periods.

In order to detail the behavior of radon's time evolution we make use of wavelet analysis. The latter consists of a localized Fourier transform by means of a wave confined, in this case, in time and with variable wavelength and amplitude. The wavelet adopted here is the classical Morlet function defined as:

$$\Psi(\eta) = \pi^{-\frac{1}{4}} e^{i\omega_0\eta} e^{-\frac{\eta^2}{2}} \tag{3}$$

where η is a non-dimensional time parameter and ω_0 is the non-dimensional frequency (assumed equal to 6 to guarantee admissibility of the function; Farge, 2000). Given the time series of radon concentration c_i with i=0, ... N-1 time spaced of δt, the wavelet transform reads:

$$W_n(s) = \sum_{n'=0}^{N-1} c_{n'} \Psi^* \left[\frac{(n' - n)\,\delta t}{s} \right], \tag{4}$$

where * indicates the complex conjugate of the wavelet function. In Eq. (4), n and s govern respectively the translation of the function along the time coordinate and the scales represented by the function. By moving the wavelet along the time dimension, it resonates with the time series c_i structures with scale s, and provides information about the signal variance, the scale and the location in time at which it occurs. By repeating the procedure for a range of scales one can obtain the so-called scalogram i.e. a three dimensional representation of the amplitude variability with scale and time. A number of aspects have to be considered when selecting the wavelet function, for its normalization and for the selection of the scale range s in relation to the time series analyzed. Herewith we refer the reader to the comprehensive description of the problem described by Torrence and Compo (1998).

Figures 3a–f show the wavelet analysis of the radon time series relating to the months of January (3a), March (3b), May (3c), July (3d), September (3e), and Oc-

tober (3f). For the sake of synthesis only these months were selected as they contain features that are also present in the others. In all plots the x-axis is time expressed in hours from the beginning of the month. The upper panel gives the time series of radon through out the month and the lower panel the corresponding scalogram. The y-axis of the scalogram refers to the time scale ranging from 2 to 200 h. The contours represent the square of the wavelet amplitude and therefore the variance or power of the signal. The contours in all scalograms of Figs. 3a–f are normalized by the global wavelet spectrum so that they can be compared with one another. Similarly to what has been done for the Fourier analysis of Fig. 2b, one can determine the 95% percent confidence that the wavelet will fall in a specific range of scales and times. The latter is obtained by means of a χ^2 test as described in Torrence and Compo (1998). The white contour superimposed to the colored ones is the 95% confidence contour. The hatched surface defines the so called cone of influence (COI), it is the region where the wavelet power drops by a factor e^{-2}. The power drop is a consequence of padding the time series with zero values at the edges in order to reach a number of components corresponding to a power of two and adopted to facilitate the wavelet analysis. The area outside the COI therefore defines the scale-time range in which the wavelet transform strictly refers to the actual time series values.

By inspection of the Figs. 3a–f one can immediately identify the differences with the power spectrum of Fig. 2b. In all scalograms the wavelet analysis identifies significant (included in the white contour) power levels in correspondence to the 24 h scale as determined by the Fourier analysis. This time the power peaks can also be related to the time coordinate. Therefore, for example in January (Fig. 3a), the diurnal variation is disrupted up until the end of the first week, while in the following week the 24 h scale is evident. During the months of March, July, September and October this feature is constantly identified. On top of the diurnal cycle which is also clearly evident by analyzing the time series, the wavelet analysis identifies relevant power contributions at lower scales. January is again an example in this respect. There is a secondary periodic contribution at 12 h which is not present in the other months and that was

globally identified by the Fourier analysis. This contribution is visible in the second week of January as a constant contour at s=10–12 h and in a more patchy way in the third and fourth weeks.

Having identified the exact location in time of occurrence of the variance maximum, one can connect it to the actual portion of the signal that generates it and therefore identify its origin. The peak is caused by the fact that the concentration grows during the night, levels off at the end of it, before it reduces during the day. This produces the appearance of a second scale in the scalogram as the night and day evolution of concentration can be clearly separated by the analysis. The 12-h period is a typical feature of January and February (not shown) and does not appear systematically in any other month of the year. By comparing the January scalogram and time series with those of the other months, one can see that in the other cases the transition between night and day trends is very sharp and therefore no additional structure beyond the diurnal cycle is identified.

The eight hours timescale identified by the Fourier analysis can also be seen in the scalogram of January. It can be connected to the nighttime boundary layer formation and evolution. In correspondence to the time range in which this scale appears we can notice:

1. A sudden increase of concentration due to the collapsing of the daytime ABL. This phase lasts between 6 to 8 h;
2. The growth of concentration between 10:00 p.m. and 08:00 a.m. of the following day with a different trend;
3. The sharp collapsing of concentration due to the rapid growth of the ABL between 09:00 a.m. and 02:00 p.m.;
4. After this phase the concentration remains at constant low levels until the cycle repeats.

Differently from other months, in January and February the change in trend between the collapse of daytime turbulence and the formation of the nocturnal stable layer is more evident and constant in time. The variation of growth rate could be connected to steady reduction of the boundary layer height occurring in the presence of a constant cooling rate at the surface (Nieuwstadt, 1981) as would be the case for January and February. In March the same feature can be noticed but it appears more sporadically. The investigation of wind speed evolution with time shows the presence of calm of wind during the night thus indicating that only micrometeorological data could allow a comprehensive explanation of the process. In general one can speculate a variation in the stable stratification during the night time hours that produces the change of slope in the concentration rate.

Below the eight-hour scale, all scalograms allow also the identification of isolated features that are connected to sudden variations of the concentration level. The scalograms indicate that the lower time scale's peaks relate to sudden increases or decreases of concentration which are randomly distributed and do not constitute a constant feature of the power spectrum as Fig. 2b seems to indicate. This is typically the case for the first week of March where the sudden decrease of concentration produces large power variations at scales ranging from 1 to 10 h and extending over a time period of approximately 30 h. When the diurnal variation is not perturbed by external events, one can notice that the majority of small scale perturbations tend to occur rather systematically during the nighttime hours either on the first phase of the concentration growth or in the second as described in (I) and (II). A clear case of such event is the nighttime occurrence of double peaks as in the case of January (Fig. 3a, 5th concentration peak from the right), July (Fig. 3c, 5th, 6th, and 10th concentration peaks from the right). The variability of concentration in these cases depends strongly on the variability of shallow nocturnal boundary layer which can be sensitive to sudden wind speed variations like the formation of low level jets. The double peak feature seems systematically connected to the 6 h scale identified by the Fourier spectrum.

ACPD
5, 12895–12937, 2005

The role of external parameters in perturbing the radon concentration can be clearly seen in May. During this month the diurnal variation disappears across the first and the second week as a consequence of a clear reduction of the concentration levels. The reason for that will be analyzed in the next section.

The wavelet analysis has identified that while the 24 h scale is a constant feature of the daily evolution of the radon concentration, the 12 and 8 h scales appear mainly in correspondence to the nighttime period when the concentration changes growth rate after the collapse of daytime turbulence and in correspondence of concentration fluctuations therein. The smallest time scales (6 and 4 h) identified by the Fourier analysis cannot be attributed systematically to specific moments of the time evolution of radon but occur randomly in the time series.

4. Wavelet analysis of meteorological variables and relationship with the radon time series

The variability of radon concentration in the atmosphere is strictly connected to the meteorological conditions as the emission from the surface is in principle constant in time and space for a given soil type (Moses et al., 1963). In this section we will analyze the dependence of radon concentration on the meteorological situation at the measuring station and we will use the wavelet analysis for all variables for a better understanding of the variables interactions.

As pointed out by several works in the past, two meteorological variables affect radon concentration in the atmosphere or more specifically in the boundary layer, namely wind speed and precipitation. The impact of varying wind speed is due to two main reasons: advection of radon free or radon rich air, increase of shear driven turbulence with consequent effective dilution of the radio nuclide and concentration reduction. For the sake of completeness also the increase of surface heat flux and convective conditions should be accounted as a cause of concentration reduction. Precipitation affects radon concentration through rain out and wash out which according to few authors can

ACPD
5, 12895–12937, 2005

remove the radio nuclide from the air (e.g. Gat et al., 1966) and mainly by reducing the exhalation flux from the surface. The presence of a water saturated layer at the surface, ice or snow cover can delay or prevent radon from being exhaled and therefore affect the emission rate. Some authors (e.g. Hatuda, 1953; Moses et al., 1963; Kranner et al., 1964) consider also atmospheric pressure variations as possibly responsible for variation of surface emissions. Namely increase (decrease) of pressure would damp (increase) the exhalation flux from the soil. As shown before, the present dataset does not show any clear feature in this respect and on the contrary a positive correlation between the pressure time evolution and that of radon concentration. For the sake of completeness it should be mentioned that the detailed studies of Guedalia et al. (1970), Clements and Wilkening (1974), Guedalia et al. (1980), Ishimori et al. (1998) and Katoaka et al. (2003), indicate that only sudden drops or increases of pressure (of the order of 10 to 15 hPa) can cause a modification of the radon emission. Such occurrences are never recorded in the present data set.

The radon time series analyzed in this study is particularly interesting since the measurements were conducted in a location and time period where low wind conditions can be generally found apart from sporadic short term events. During 1997 few precipitation events were recorded and mainly concentrated in short-term intense rain periods. Such information combined with the wavelet analysis allows us to clearly identify the effect of these parameters on the radon concentration and the analysis of the scale interactions.

An interesting case is presented in Fig. 4. The figure shows the time evolution of wind speed, precipitation and radon concentration measured at the EMEP station in May 1997. Each time series in the figure is presented together with the corresponding wavelet analysis. The scalogram of wind speed identifies the presence of the 24 h periodicity connected to local breeze event typical of the region and smaller scale variability. As one can see from the time series, wind speeds are relatively small. During the whole month only three major precipitation events occurred, for a total of 77 mm of rain. A peak of 20 mm can be noticed in the first week (56.8 mm in the first 300 h)

ACPD
5, 12895–12937, 2005

and during the third and fourth week two short and less intense precipitation events took place. The constant diurnal variation of radon time series of the first four days of the first week is sensibly affected by the first precipitation event. The diurnal periodicity is disrupted; the concentration reduces to a half of the original average value for the following eight days. The analysis of the precipitation time series does not allow one to attribute directly the radon periodicity disruption to the precipitation event as the first extends far beyond the occurrence of the precipitation. However the inspection of the precipitation scalogram indicates a qualitative correspondence between the scales associated to the precipitation event and the perturbation of the radon time series. In the figure, the two vertical dashed lines indicate the time range of extension of significant scale of the precipitation. As one can see it corresponds to the period of time over which the radon periodicity is perturbed. Beyond this time period the radon time series shows again the typical diurnal variation. The radon periodicity disruption can confidently be attributed mainly to precipitation. The wind speed in the time period highlighted by the two vertical lines is in fact comparable to the one present in other parts of the time series where radon shows the diurnal variation.

A case similar to the one of May is found in September as shown in Fig. 5. In this case, however, the effect of the precipitation on the radon concentration periodicity is reduced due to a smaller amount of precipitation fallen. The precipitation event reduces the amount of concentration in air but does not perturb the diurnal evolution as can be seen from the time series and the corresponding variance in the scalogram. A remarkable feature, also noticed in previous studies (Israel et al., 1966), is the response time of radon exhalation and therefore concentration to the start and end of the precipitation event. Ishimori et al. (1998) determine a recovery time of the exhalation flux of 1.5 days after a precipitation event of 15 mm. Israel et al. (1966) found a comparable reduction due to precipitation events of less than 3 h and rate above 3 mm/h. Megumi and Mamuro (1973) found a reduction of the ground exhalation rate of a factor 2 after a precipitation event of 93 mm.

The sensitivity of radon exhalation and concentration to small amounts of precipita-

ACPD
5, 12895–12937, 2005

tion, also evident in the present dataset, points clearly towards the need of a parameterization of the process within global models (e.g. Jacob et al., 1997; Dentener et al., 1999; Josse et al., 2004). The latter in fact normally consider uniform fluxes in space and time and do not account for the flux dependence on precipitation. For an appropriate description of radon distribution in the atmosphere, its response to the latitudinal, time and intensity variability of precipitation should be accounted for explicitly.

The combined effect of wind speed and precipitation on radon concentration is shown in Fig. 6. Across the second and the third week of December (highlighted by the two vertical dashed lines) one notices a build up of wind intensity with scales ranging from 1 h to 10–24 h which gives room later on to a precipitation event of reduced intensity and with comparable time scales. The effect on the radon concentration can immediately be evinced from the time series.

An interesting case, though different from the ones analyzed so far, relates to July and is presented in Figs. 7a and b. In Fig. 7a, during the first week wind speed increases consistently and suddenly over a time scale of 12–15 h while a precipitation event takes place with a scale ranging from 1 to 100 h. During the corresponding period of time radon concentration does not show any distinctive pattern apart from a sudden peak occurring during the wind intensity maximum period (highlighted by the black dotted line). This peak represents an anomaly also considering the scale and the intensity of the precipitation event. The analysis of other variables such as relative humidity and NO_x concentration (Fig. 7b) leads us to conclude that the peak is probably due to the advection of an air mass with high concentration of radon that went past the monitor. The radon peak in fact corresponds to a sudden and very large peak of NO_x (middle panel) which passes during the intense wind period from few tens of ppb to 150 ppb thus indicating the transport of the tracer from a NO_x rich region. The radon peak could very likely be connected to the same advection process.

ACPD

5, 12895–12937, 2005

5. Estimate of the radon surface flux from concentration time series

The analysis of the time series of the various months outlines the presence of specific periods during which the radon concentration behaves in a special way. This is typically the case of August, September and October. Figures 8a and b refer to the case of October. The upper panel shows the time series of radon concentration during the whole month. The part of the plot that is not hatched is the period of interest in this analysis. The plot also shows the time evolution of precipitation as one of the governing factors, together with wind speed, of radon concentration as shown before. In the time window highlighted, no precipitation event occurs and the wind speed ranges below $1\,ms^{-1}$. Between the 250th and 300th hour, a sharp decrease in radon concentration occurs coinciding with a period with high wind speeds ranging between 3 to $4\,ms^{-1}$ but stopping at hour 331. From that moment on and for the following 6 days, the radon concentration shows the usual daily evolution though superimposed to a linear growth. Similar cases are found in September (2 sequences Fig. 9a–c) and August (Fig. 10a–b). All the time series indicate a build up of radon in the boundary layer that occurs for more than two consecutive days. The well-behaved character of such occurrences, which are the only ones found through out the year, can easily be spotted by simple inspection of the time series. In all portions, the maximum and minimum concentration increase linearly from one day to the other.

The absence of precipitation events in the selected periods leads to the conclusion that the exhalation rate of radon from the ground is constant. The absence of significant wind speeds and the inspection of NO_x concentration, lead to excluding advection of radon from other areas. One can therefore deduce that the radon build up is connected to a rather regular boundary layer excursion and a negligible detrainment of radon at boundary layer top.

The daily average concentration has been calculated for the various periods and a linear fitting has been obtained as depicted in Figs. 8b, 9b–c and 10b. In spite of the different months, all the linear fitting show a common slope value, namely 0.11 in

October; 0.091 and 0.092 in September; 0.11 in August. The linear growth of concentration superimposed to the daily evolution is also used by Vinod Kumar et al. (1999) to validate their one-dimensional model.

The results of this analysis are used herewith for a crude calculation of the surface flux of radon. It should be specified that this might be different from the actual exhalation flux which occurs at the direct surface, but it rather represents an estimate of the turbulent flux in the first portion of atmospheric surface layer.

The time evolution of radon concentration can be written as:

$$\frac{dC}{dt} = -\frac{(F_H - F_S)}{H} - \lambda C, \tag{5}$$

where, the vertical divergence of the turbulent flux has been approximated by the ratio of the net flux (given as difference between the flux at the surface layer top F_H, and that at the bottom F_s), and the boundary layer depth, H. In other words Eq. (5) is a bulk expression for the boundary layer which is represented as a layer of depth H with a radon in-flux at the surface and an out-flux at the top. In Eq. (5) λ is the decay frequency (equal to log(2)/3.8 day^{-1}).

In this context we assume that:

$$F_H \ll F_s, \tag{6}$$

as justified by the concentration build up in the absence of external factors that could perturb the surface emission. Equation (6) thus assumes a negligible entrainment of radon-free air and detrainment of radon at the boundary layer top.

The analytical solution of Eq. (5) reads:

$$C = C_0 e^{-\lambda(t-t_0)} + \frac{F}{\lambda H}\left(1 - e^{-\lambda(t-t_0)}\right) \tag{7}$$

By Taylor expansion of the exponential relationship, Eq. (7) can be linearized to:

$$C = C_0\left[1 - \lambda t + o(t^2)\right] + \frac{F}{\lambda H}\left[\lambda t + o(t^2)\right] \tag{8}$$

where t_0 has been assumed equal to 0. By neglecting the higher order terms and re-arranging the expression, Eq. (8) reduces to:

$$C = \left(\frac{F}{H} - C_0\lambda\right) t + C_0 \tag{9}$$

The linear interpolation of the time evolution of concentration given in Figs. 8–10, provides the following expression:

$$C = mt + C_0 \tag{10}$$

where m=0.1 Bqm^{-3} h^{-1}. In order to retrieve the magnitude of the flux at surface we can equate the slope of Eq. (9) and that of Eq. (10):

$$F = mH + \lambda C_0 \tag{11}$$

Considering that a bulk value for the boundary layer depth (H) can be confidently assumed of order $10^2 m$, for all time periods and the considered location and that C_0 is order 1, Eq. (11) reads:

$$F \approx \left(\frac{1}{360} + \frac{10^2 \log(2)}{3.8 * 24 * 3600}\right) \frac{Bq}{sm^2}, \tag{12}$$

which reduces to:

$$F \approx (0.0022)\, \frac{Bq}{sm^2} \tag{13}$$

The order of magnitude of F is well within the ranges directly measured in several other locations with characteristics similar to the EMEP station at JRC (e.g. Guedalia et al., 1970; Kataoka et al., 2001; Levin et al., 2002). It should be noticed that in Eq. (12) the dominant term is mH which is an order of magnitude larger than the second one.

The order of magnitude of the flux, determined by the previous analysis, is then used to reproduce the portion of time series depicted in Figs. 8–10. The only free parameter in Eq. (7) is H, however starting from the regular behavior of the concentration

ACPD
5, 12895–12937, 2005

in time, we assume the surface layer depth varying as a sinus function and having an excursion from 40 to 260 m during night and day, respectively. The solution of Eq. (5) with the use of a time varying H and a flux value of 0.005 Bqm^{-2} s^{-1} gives the result shown in Fig. 11. The figure shows that the flux estimate and Eq. (7) are able to reproduce the linear growth of the radon concentration. Small variability of maximum and minimum concentration values are obviously connected to the crude representation of the boundary layer depth evolution which according to the expression used assumes always the same maximum and minimum values while in reality one expects more variability within the range of values assumed. In time, if no external event would occur to perturb the radon emission and boundary layer evolution, the concentration growth rate would reduce to zero as the emission would compete at one stage with radioactive decay.

6. Conclusions

A one-year time series of radon-222 collected in 1997 in the North of Italy has been studied. The time series is particularly interesting as it was collected in region and time period where meteorological events controlling the radon concentration in air were moderate in intensity and sporadic.

Given the time variability of radon concentration in air, wavelet analysis was used to better identify feature that the classical Fourier analysis would only provide globally. The latter has in fact identified the presence of dominant time scales in the time series that range from 4 to 24 h but that cannot be associated to specific occurrences in time. Through wavelet analysis however, the energy corresponding to scales smaller than 24 h where precisely connected to specific portions of the time series. In such a way a more clear identification of the processes leading to the occurrence of the specific timescale was made. The role of wind speed and precipitation in controlling the radon variability in time was also investigated by means of the wavelet analysis. The most important finding is the correlation between the timescale identified by the latter and

ACPD
5, 12895–12937, 2005

the effect on the radon concentration even in the case of short term precipitation events or periods of intense wind. Once more wavelet analysis has proven to be a very useful investigation tool in the case of environmental variables.

Specific time periods within different months of the year that identified concentration build up in the surface layer were analyzed more in detail. The concentration growth rate was found to be the same regardless of the different months and seasons thus indicating a common behavior of radon dispersion in the region. The growth rate was then used to obtain an estimate of the radon surface flux which is matching the findings of more detailed studies.

Radon-222 is once more demonstrated to be an excellent tracer for boundary layer studies. The well-behaved character of surface emission and the effect of precipitation and boundary layer turbulence, make it a perfect candidate for atmospheric dispersion analysis and characterization. The availability of micro meteorological measurements in combination to radon concentration and flux data would allow an even deeper investigation of radon dispersion and boundary layer properties. Future investigation will be dedicated to determining the effect of precipitation intensity on the radon surface flux and surface layer concentration. Special attention will also be given to the open question of the role of atmospheric pressure variations on radon emission.

Acknowledgements. The author is grateful to B. Ottobrini that has originally collected the radon data. To M. De Cort (JRC/IES, I) and J. Vilà-Guerau de Arellano (WAU, NL) for the fruitful discussions during the preparation of this work. M. G. Marcazzan and U. Facchini (University of Milan, I) are thanked for providing additional data, literature information and fruitful discussions based on their long experience on the radon issue. The contribution of J. P. Putaud (JRC/IES, I) is also acknowledged for the provision of meteorological data collected at the EMEP station during the radon sampling campaign.

References

Attié, J. L. and Durand, P.: Conditional wavelet technique applied to aircraft data measured in the thermal internal boundary layer during sea-breeze events, Bound. Layer Meteorol., 106,

359–382, 2003.
Beck, H. L. and Gogolak, C. V.: Time dependent calculations of the vertical distribution of ^{222}Rn and its decay products in the atmosphere, J. Geophys. Res., 86(6), 3139–3148, 1979.
Beran, M. and Assaf, G.: Use of isotropic decay rates in turbulent dispersion studies, J. Geophys. Res., 73(27), 5297–5295, 1970.
Clements, W. E. and Wilkening, M. H.: Atmospheric pressure effects on ^{222}Rn transport across the Eatrth-Air Interface, J. Geophys. Res., 79, 5025–5029, 1974.
Dentener, F., Feichter, J., and Jeuken, A.: Simulation of the transport of Rn^{222} using on-line and off-line global models at different horizontal resolutions: a detailed comparison with measurements, Tellus, 51B, 573–602, 1999.
Druilhet, A. and Fontan, J.: Utilisation du thoron pour la détermination du coefficient vertical de diffusion turbulente près de sol, Tellus, 25, 199–212, 1973.
Druilhet, A., Attié, J. L., de Abreu Sá, S., Durand, P., and Bénech, B.: Experimental study of inhomogeneous turbulence in the lower troposphere by wavelet analysis. Wavelets: theory, algorithms, and its applications, edited by: Chui, K., Montefusco, L., and Puccio, L., pp. 1–17, 1994.
Facchini, U., Sesana, L., Milesi, M., De Saeger, E., and Ottobrini, B.: A year's radon measurements in Milan and at EMEP station in Ispra (Lake Maggiore, Italy), Air pollution Conference (VII), edited by: Brebbia, C. A., Jacobson, M., and H. Power, ISBN 1-85312-693-4: 1112, 1999.
Farge, M.: Wavelet transform and their application to turbulence, Annu. Rev. Fluid. Mech., 24, 395–457, 2000.
Farge, M. and Schneider, K.: Analysing and computing turbulent flows using wavelets. New trends in turbulence, Les Houches 2000, Vol. 74, edited by: Lesieur, M., Yaglom, A., and David, F., 449–503, Springer, 2002.
Galmarini, S. and Attié, J.-L.: Turbulent transport at the thermal internal boundary-layer top: wavelet analysis of aircraft measurements, Bound. Layer Meteorol., 94, 175–196, 2000.
Gao, W. and Li, B. L.: Wavelet analysis of coherent structures at the atmosphere forest interface, J. Appl. Meteorol., 32, 1717–1725, 1993.
Gat, J. R., Assaf, G., and Miko, A.: Disequilibrium between short-lived radon daughter products in the lower atmosphere resulting from their washout by rain, J. Geophys. Res., 71, 1525–1535, 1966.
Gilman, D. L., Fuglister, F. J., and Mitchell Jr., J. M.: On the power spectrum of "red noise", J.

ACPD
5, 12895–12937, 2005

Atmos. Sci., 20, 182–184, 1963.
Guedalia, D., Laurent, J.-L., Fontan, J., Blanc, D., and Druilhet, A.: A study of Radon 220 emanation from soil, J. Geophys. Res., 75, 357–369, 1970.
Guedalia, D., Ntsila, A., Druihlet, A., and Fontan, J.: Monitoring of the atmospheric stability above an urban suburban site using sodar and radon measurements, J. Appl. Meteorol., 19, 839–848, 1980.
Hatuda, Z.: Radon content and its change in soil air near the ground surface, Mem.Coll. Sci., Univ. Kyoto, Japan, Ser. B, 20, 4, 285–306, 1953.
Ikebe, Y. and Shimo, M.: Estimation of the vertical turbulent diffusivity from thoron profiles, Tellus, 24, 29–37, 1972.
Ishimori, Y., Ito, K., and Furuta, S.: Environmental effect of radon from Uranium Waste rock piles: Part I – Measurements by passive and continuous monitors, in: Proceedings of the 7th Tohwa University International Symposium on radon and Thoron in the Human Environment, 23-25 October, 1997, edited by: Katase, A. and Shimo, M., Fukouka, Japan, pp. 282–287, 1998.
Israël, H. and Horbert, M.: Results of continuous measurements of radon and its decay products in the lower atmosphere, Tellus, 18, 2, 638–641, 1966.
Kataoka, T., Yunoki, E., Shimizu, M., et al.: A study of the atmospheric boundary layer using radon and air pollutants as tracers, Bound. Layer. Meteorol., 101, 131–155, 2001.
Kataoka, T., Yunoki, E., Shimizu, M., et al.: Concentrations of ^{222}Rn, its short-lived daughters and ^{212}Pb and their ratios under complex atmospheric conditions and topography, Bound. Layer Meteorol., 107, 219–249, 2003.
Kranner, H. W., Schroeder, G. L., and Evans, R. D.: Measurements of the effects of atmospheric variables on Rn-222 flux and soil gas concentration, in The Natural radiation Environment, pp. 191–215, University of Chicago press, Chicago, Ill., 1964.
Kristensen, L., Andersen, C. E., Jørgensen, H. E., Kirkegaard, P., and Pilegaard, K.: First-Order Chemistry in the Surface-Flux Layer, J. Atmos. Chem., 27, 3, 249–269, 1997.
Jacob, D. J., Prather, M. J., Rasch, P. J., et al.: Evaluation and intercomparison of global atmospheric transport models using 222Rn and short-lived tracers, J. Geophys. Res., 102, 5953–5970, 1997.
Josse, B., Simon, P., and Peuch, V. H.: Radon global simulations with the multiscale chemistry and transport model MOCAGE, Tellus, 56B, 339–356, 2004.
Levin, I., Born, M., Cuntz, M., Langerdörfer, U., Mantsch, S., Naegler, T., Schmidt, M., Varlagin,

A. , Verclas S., and Wagenbach, D.: Observations of atmospheric and soil exhalation rate of radon-222 at a Russian forest site, Technical approach and deployment for boundary layer studies, Tellus B, 54, 5, 462–475, 2002.
Leyendecker, W., Brun, C., Geiss, H., and Rembges, D.: Activity of JRC EMEP Station: 1997 annual report, EUR 18084 EN, 1998.
Nieuwsdtat, F.: A rate equation for the nocturnal boundary layer height, J. Atmos. Sci., 38, 1418–1428, 1981.
Marcazzan, M. G., Rodella, C. A., and Artesani, R.: Misure della concentrazione di radon in aria esterna come indicatore della diffusione nei bassi strati dell'atmosfera, Fisica, Istituto Lombardo, B B127, 127–247, 1993.
Marcazzan, M. G. and Persico, F.: Valutazione dell'altezza dello strato rimescolato a Milano dall'andamento della concentrazione di 222Rn in atmosfera, Ingegneria Ambientale, 26, 419–427, 1996.
Megumi, K. and Mamuro, T.: Radon and Thoron exhalation from the ground, J. Geophys. Res., 78(11), 1804–1808, 1972.
Moses, H., Lucas Jr., H. F., and Zerbe, G. A.: The effect of meteorological variables upon Radon concentration three feet above ground, J. Air Poll. Control Assoc., 13, 1, 13–19, 1963.
Pearson, J. E. and Moses, H.: Atmospheric Radon-222 concentration variation with height and time, J. App. Meteorol., 5, 175–181, 1966.
Salmod, J. A.: Wavelet analysis of intermittent turbulence in a very stable nocturnal boundary layer: implications for the vertical mixing of ozone, Bound. Layer Meteorol., 114, 463–488, 2005.
Sesana, L., Caprioli, E., and Marcazzan, G. M.: Long period study of outdoor radon concentration in Milan and correlation between its temporal variations and dispersion properties of atmosphere, J. Env. Radioact., 65, 147–160, 2003.
Sesana, L., Polla, G., and Facchini, U.: Misure di radon outdoor: turbolenza e stabilita' atmosferica nella citta' di Milano e in un sito della Pianura Padana, Ing. Amb., 34, 3/4, 169–179, 2005.
Torrence, C. and Compo, G. P.: A practical guide to wavelet analysis, Bull. Amer. Meteor. Soc., 79, 1, 61–78, 1998.
Vinod Kumar, A., Sitaraman, V., Oza, R. B., and Krishamoorthy, T. M.: Application of a numerical model for the planetary boundary layer to the vertical distribution of radon and its daughter products, Atmos. Environ., 33, 4717–4726, 1999.

Zahorowski, W., Chambers, S. D., and Henderson-Sellers, A.: Ground based radon-222 observations and their application to atmospheric studies, J. Env. Radioact., 76, 3–33, 2004.

Table 1. Variable measured together with ^{222}Rn and correlation of all variables to radon concentration from the hourly data series.

	Variable	Correlation with radon
1	Wind speed	−0.457984
2	Wind direction	–
3	Temperature	−0.477703
4	Relative Humidity	0.634650
5	Precipitation	−0.0610427
6	Pressure	0.258573
7	NO_x	0.416235
8	Radon	1

ACPD

5, 12895–12937, 2005

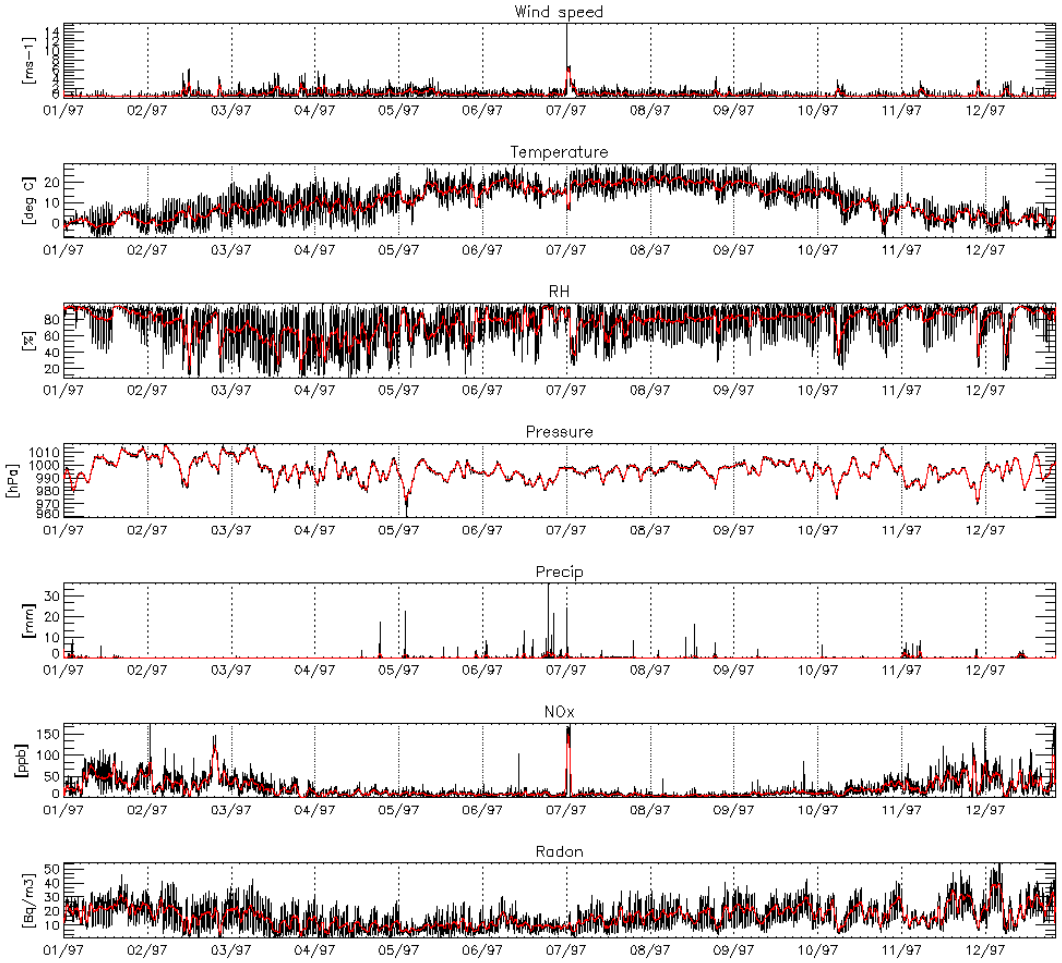

Fig. 1. Time series of wind speed, temperature, relative humidity, pressure, NO_x and Radon-222 concentration measured during 1 year at the EMEP station. The red line represents a 24 h running mean.

ACPD
5, 12895–12937, 2005

^{222}Rn concentration in the atmospheric surface layer

S. Galmarini

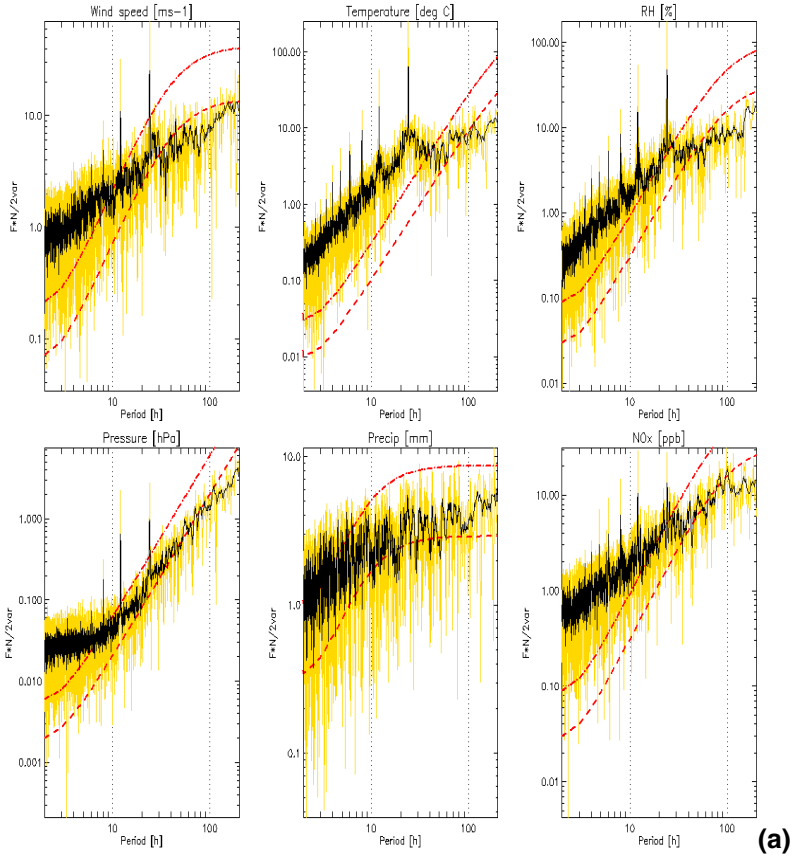

Fig. 2. **(a)** (yellow curves) Normalized power spectrum of wind speed, temperature, relative humidity, pressure, precipitation and NO_x, as a function of period expressed in hours; (black curves) 12 h running mean. **(b)** Same as (a) but for radon concentration. The red long-dashed line in (a) and (b) represents the red noise spectrum described in Eq. (1) in the text and the dot-dashed line the 95% confidence spectrum.

ACPD
5, 12895–12937, 2005

^{222}Rn concentration in the atmospheric surface layer

S. Galmarini

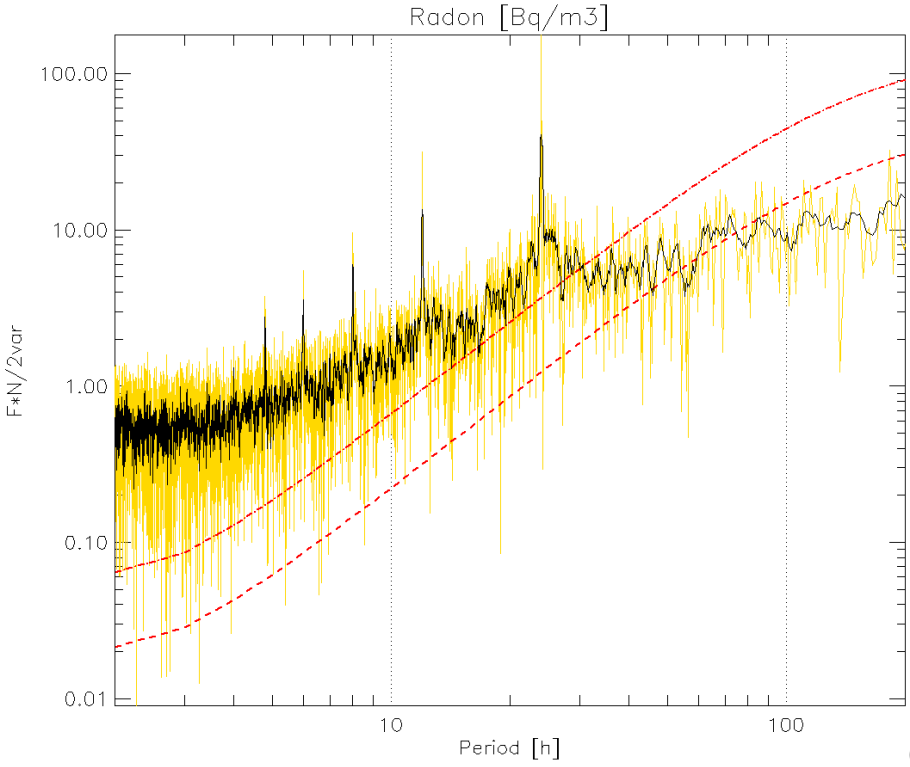

Fig. 2. Continued.

ACPD
5, 12895–12937, 2005

^{222}Rn concentration in the atmospheric surface layer

S. Galmarini

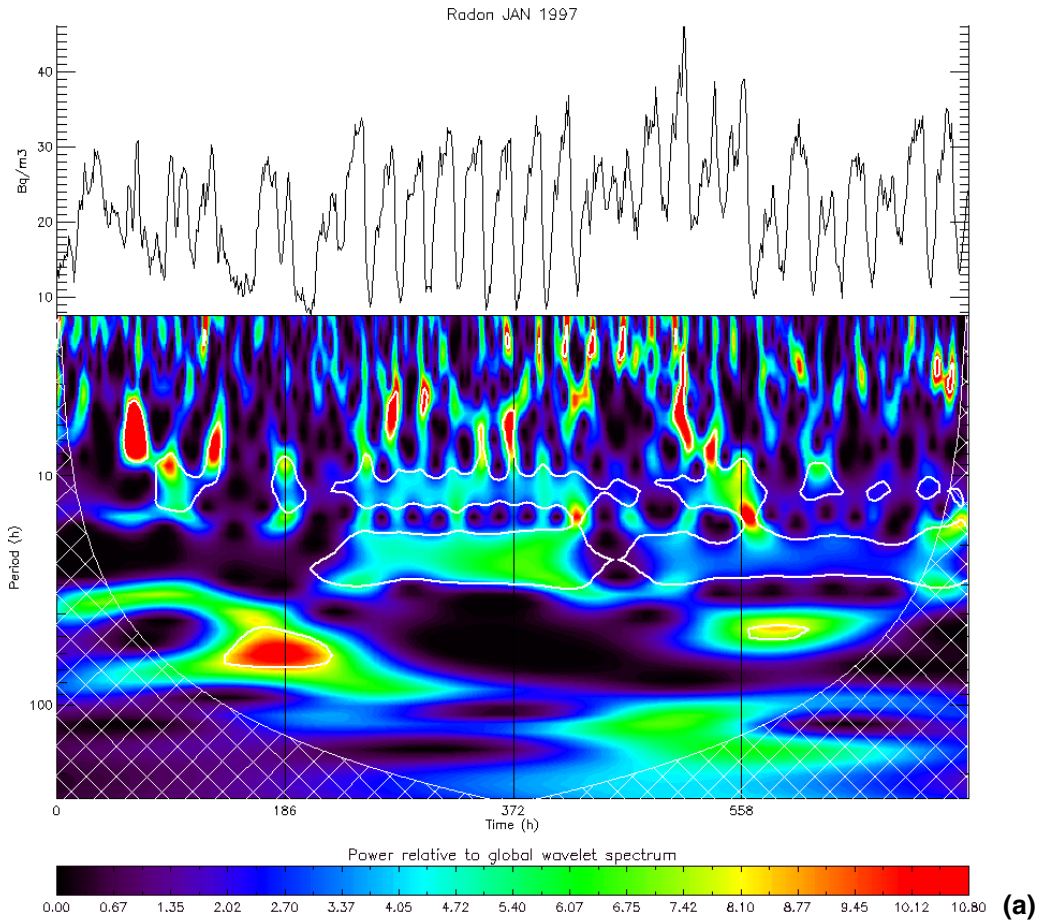

Fig. 3. Time series and scalograms of radon concentration for January **(a)**, March **(b)**, May **(c)**, July **(d)**, September **(e)**, and October **(f)** 1997. The black rectangles in figure 3d correspond to periods with missing data. With contour 95% confidence contour. Hatched surface Cone of Influence, see text for details.

ACPD
5, 12895–12937, 2005

^{222}Rn concentration in the atmospheric surface layer

S. Galmarini

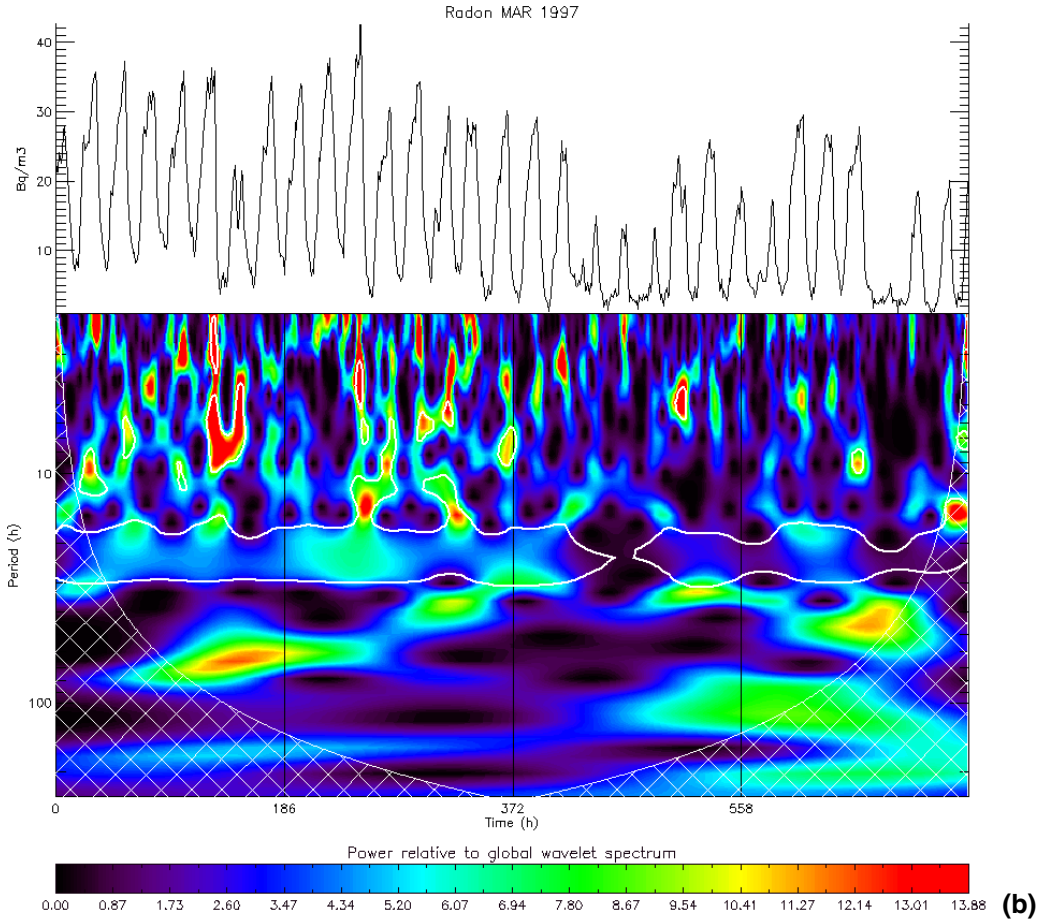

(b)

Fig. 3. Continued.

ACPD

5, 12895–12937, 2005

^{222}Rn concentration in the atmospheric surface layer

S. Galmarini

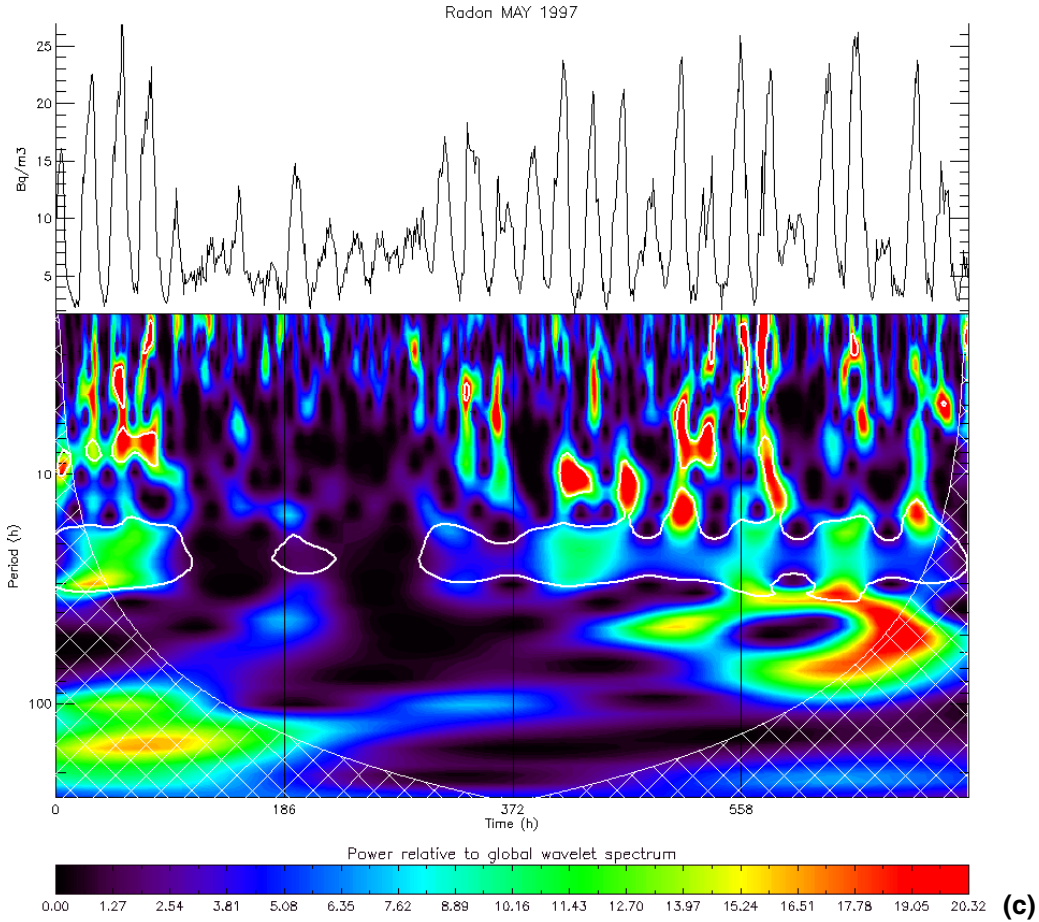

(c)

Fig. 3. Continued.

ACPD
5, 12895–12937, 2005

^{222}Rn concentration in the atmospheric surface layer

S. Galmarini

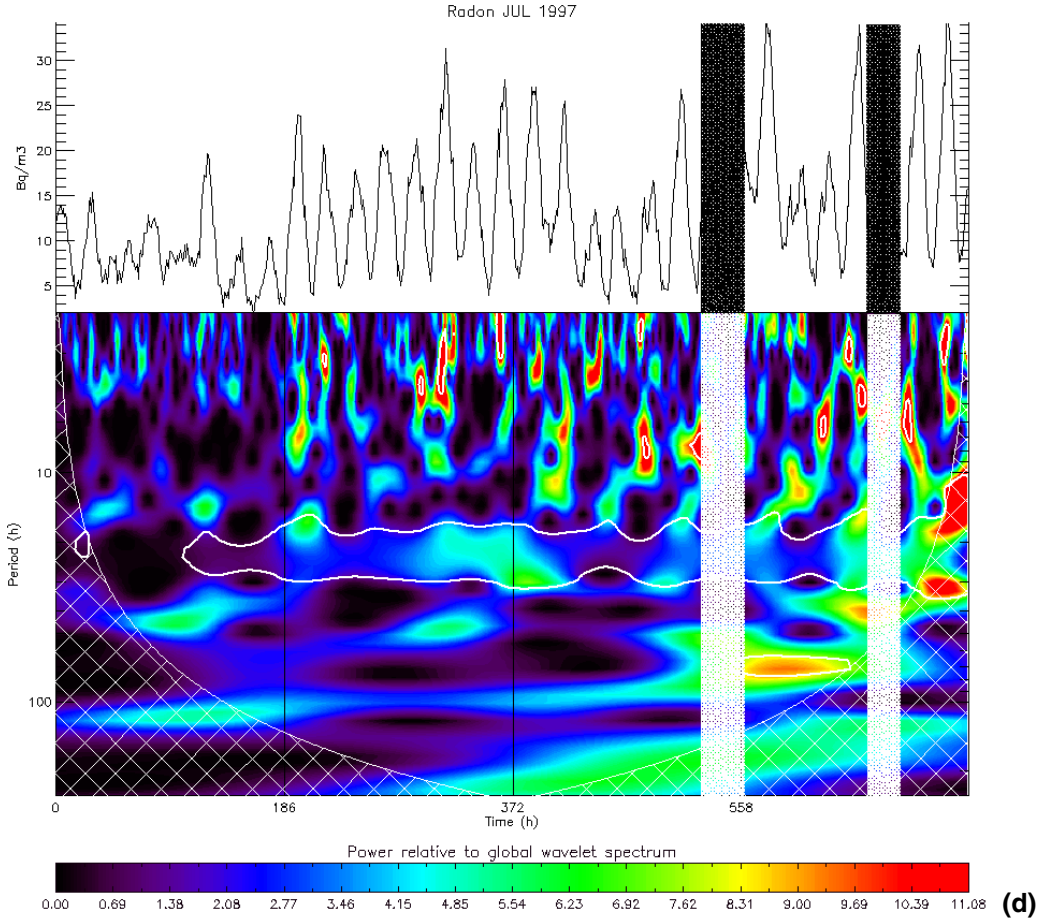

(d)

Fig. 3. Continued.

ACPD
5, 12895–12937, 2005

^{222}Rn concentration in the atmospheric surface layer

S. Galmarini

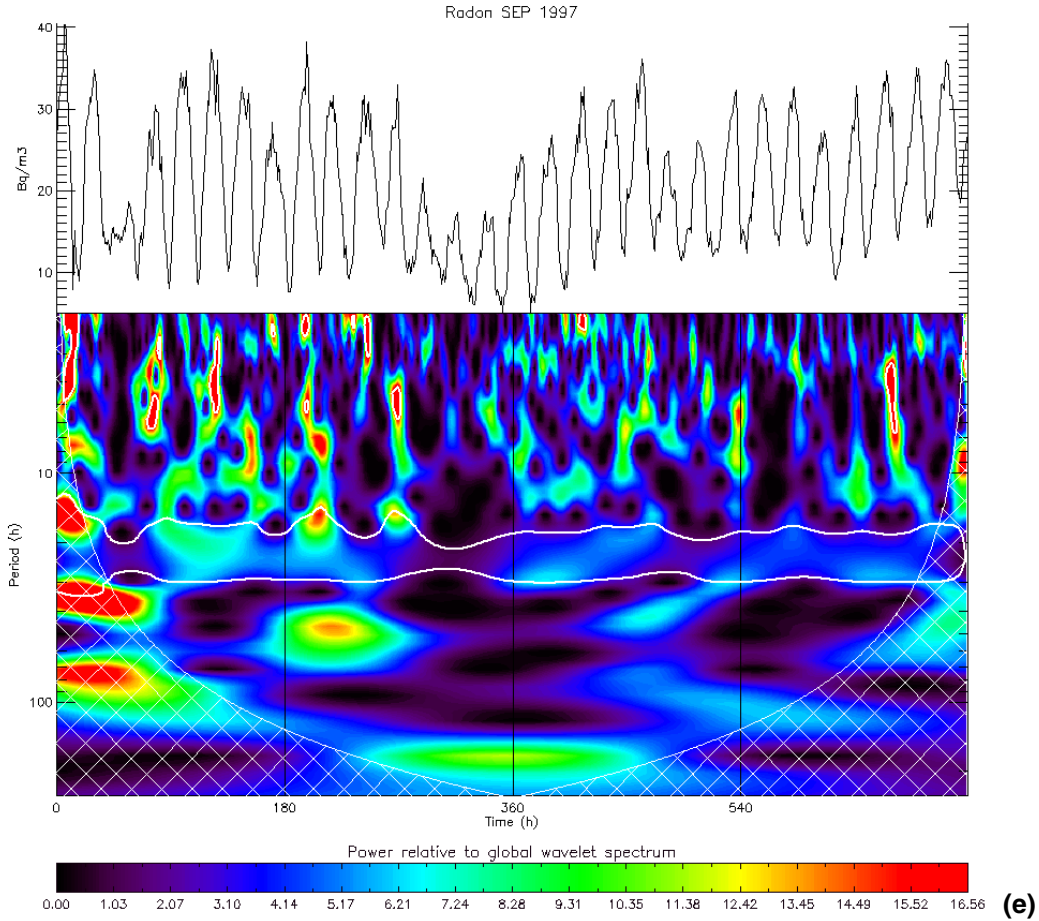

(e)

Fig. 3. Continued.

ACPD

5, 12895–12937, 2005

^{222}Rn concentration in the atmospheric surface layer

S. Galmarini

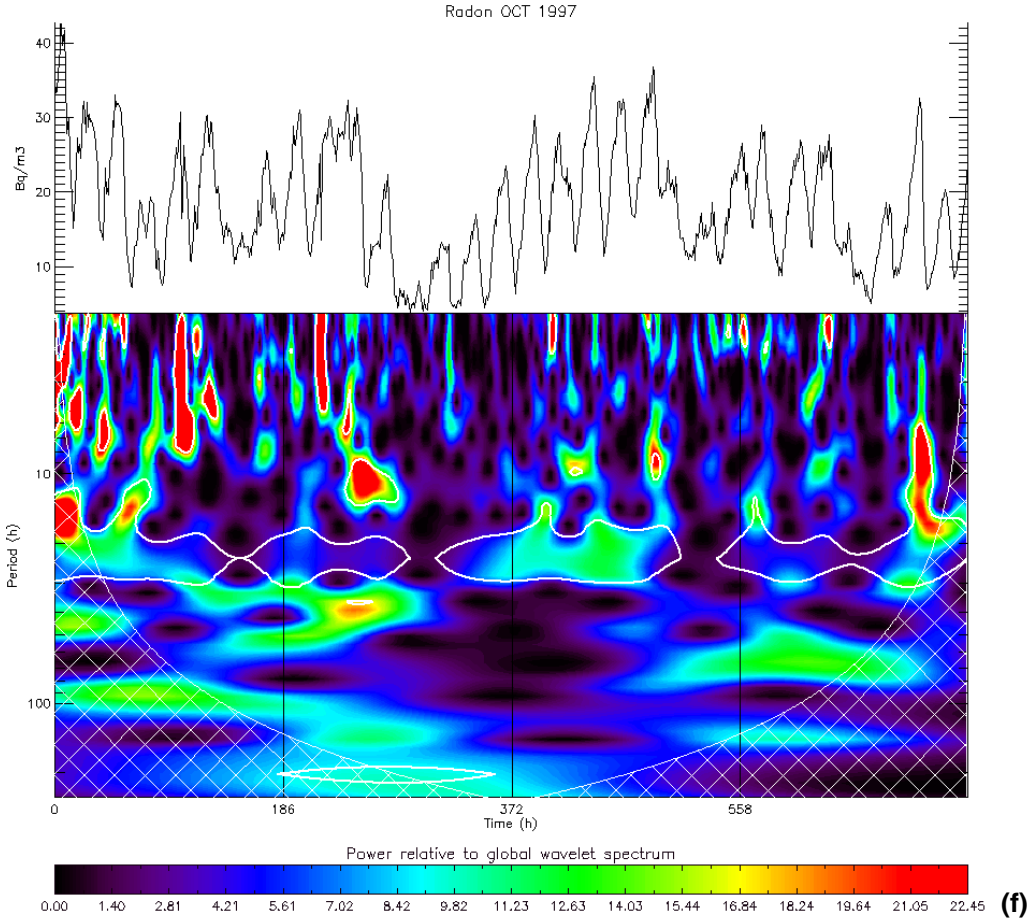

Fig. 3. Continued.

ACPD
5, 12895–12937, 2005

^{222}Rn concentration in the atmospheric surface layer

S. Galmarini

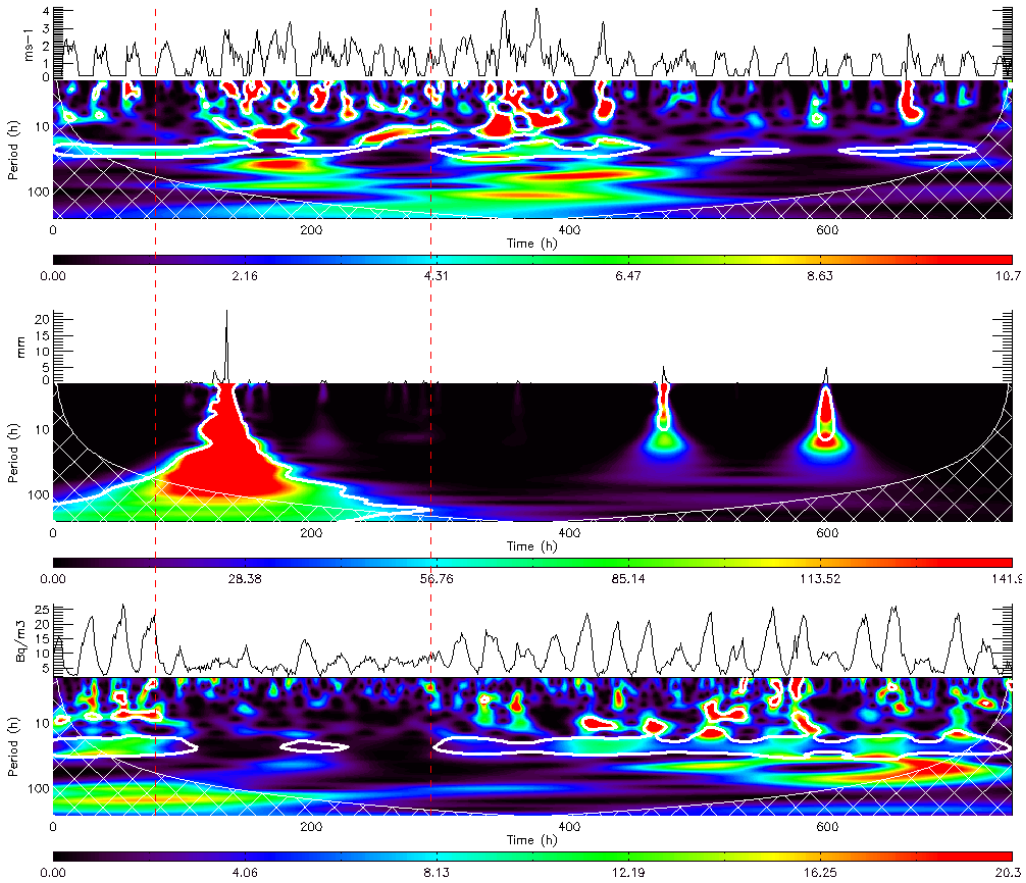

Fig. 4. Time series of wind speed, precipitation, radon and corresponding scalograms for the month of May 1997. In the scalograms the white thick contour indicates 95% confidence level and the hatched surface the COI (see text). The two vertical dashed lines are explained in the text. Color bar shows wavelet power relative to global wavelet spectrum.

ACPD
5, 12895–12937, 2005

^{222}Rn concentration in the atmospheric surface layer

S. Galmarini

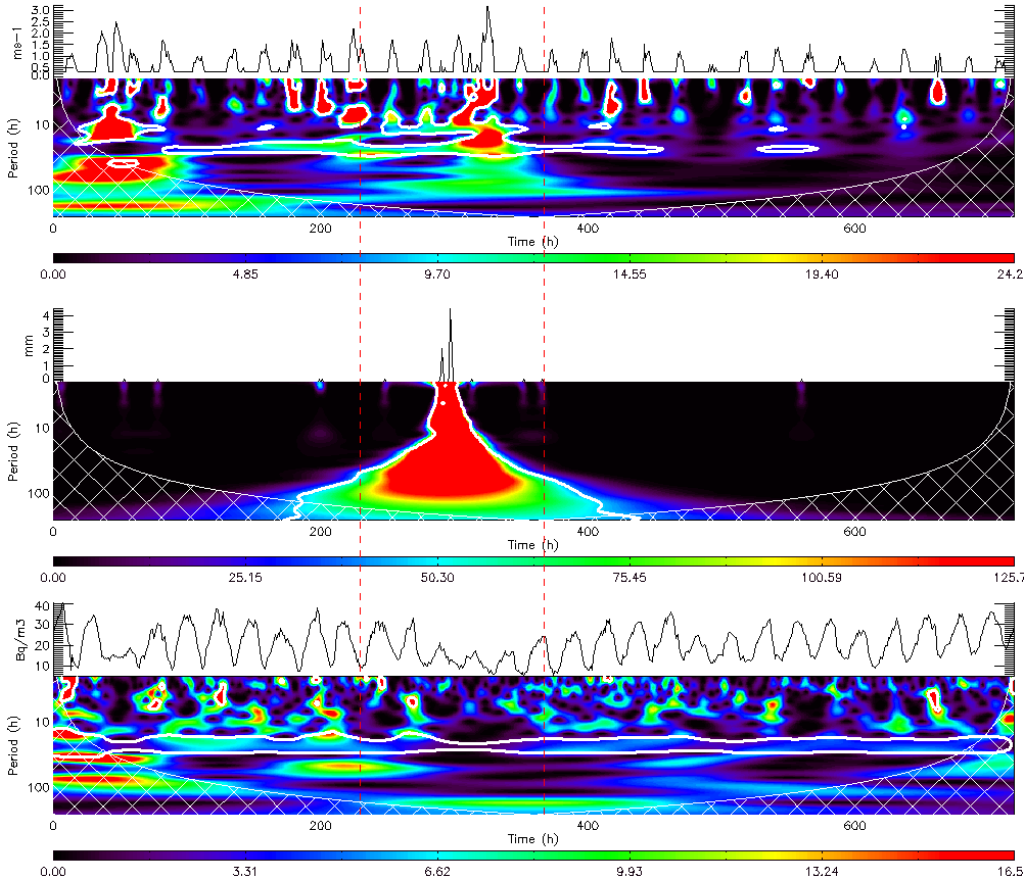

Fig. 5. Time series of wind speed, precipitation, radon and corresponding scalograms for the month of September 1997. In the scalograms the black contour indicates 95% confidence level and the hatched surface the COI. The two vertical dashed lines are explained in the text. Color bar shows wavelet power relative to global wavelet spectrum.

ACPD
5, 12895–12937, 2005

^{222}Rn concentration in the atmospheric surface layer

S. Galmarini

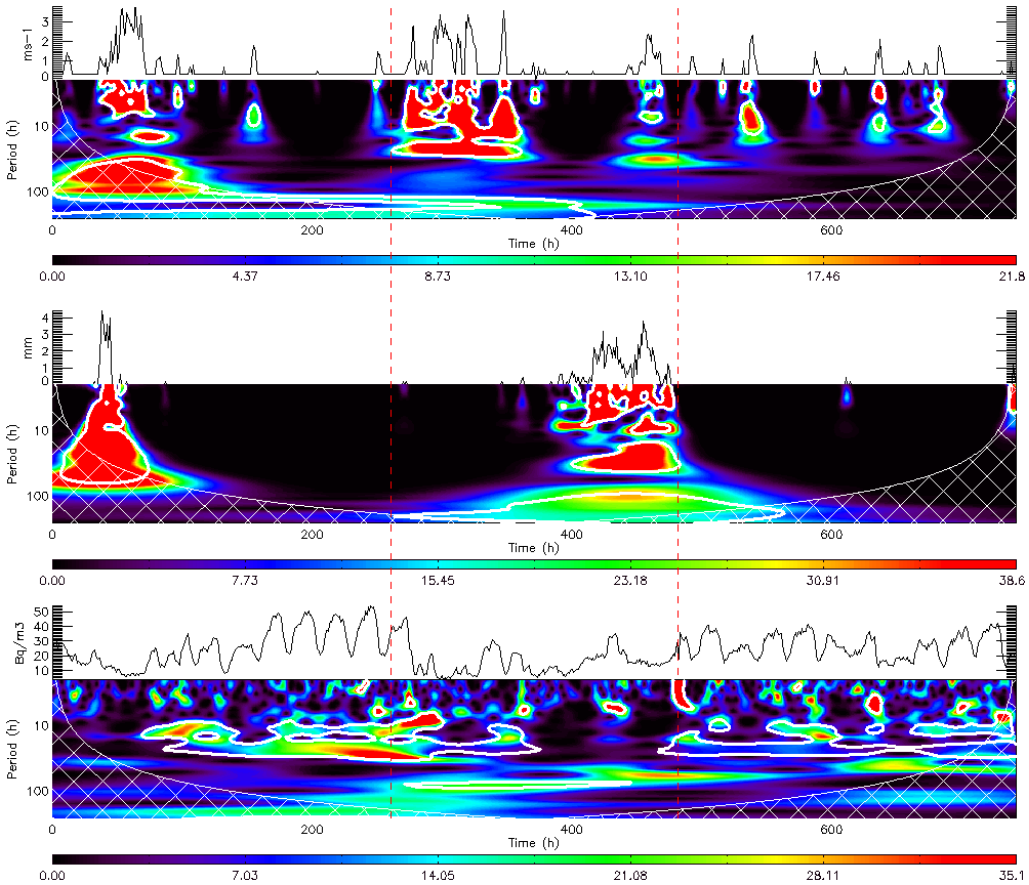

Fig. 6. Same as 5 for the month of December 1997.

ACPD
5, 12895–12937, 2005

^{222}Rn concentration in the atmospheric surface layer

S. Galmarini

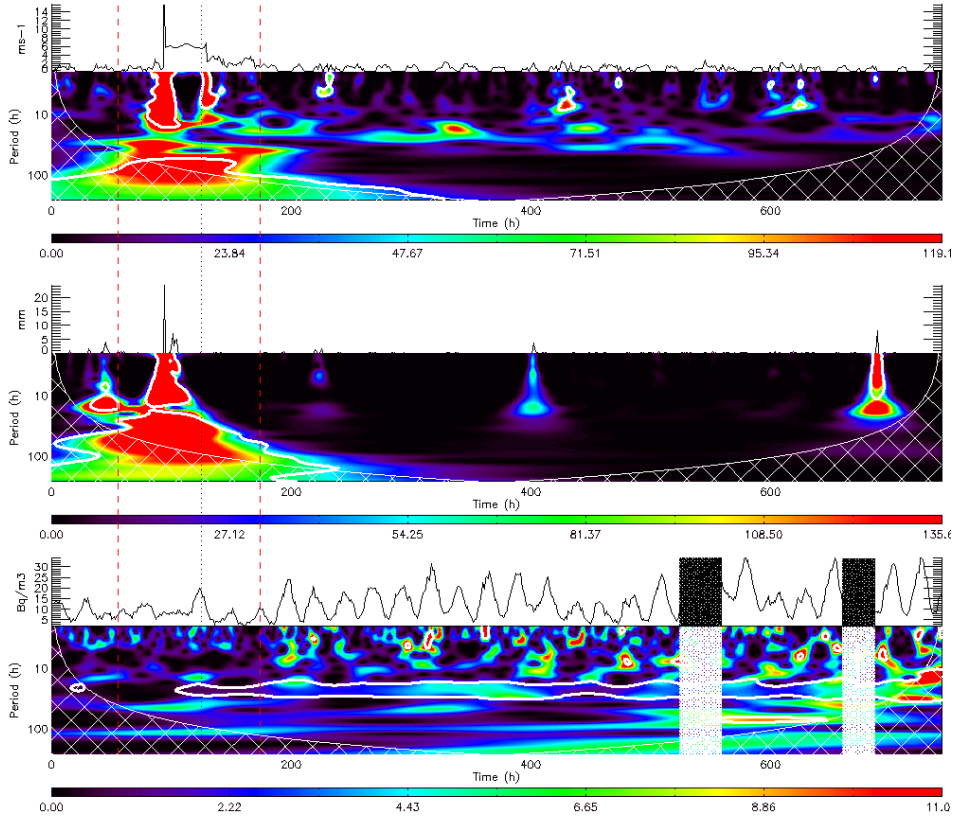

Fig. 7. **(a)** Time series of wind speed, precipitation, radon and corresponding scalograms for the month of July 1997. **(b)** Time series of relative humidity NO_x, radon and corresponding scalograms for the month of July 1997. In the scalograms the white thick contour indicates 95% confidence level and the hatched surface the COI (see text). The three vertical dashed lines are explained in the text. The black rectangles in the radon time series correspond to periods with missing data. Color bar shows wavelet power relative to global wavelet spectrum.

ACPD
5, 12895–12937, 2005

^{222}Rn concentration in the atmospheric surface layer

S. Galmarini

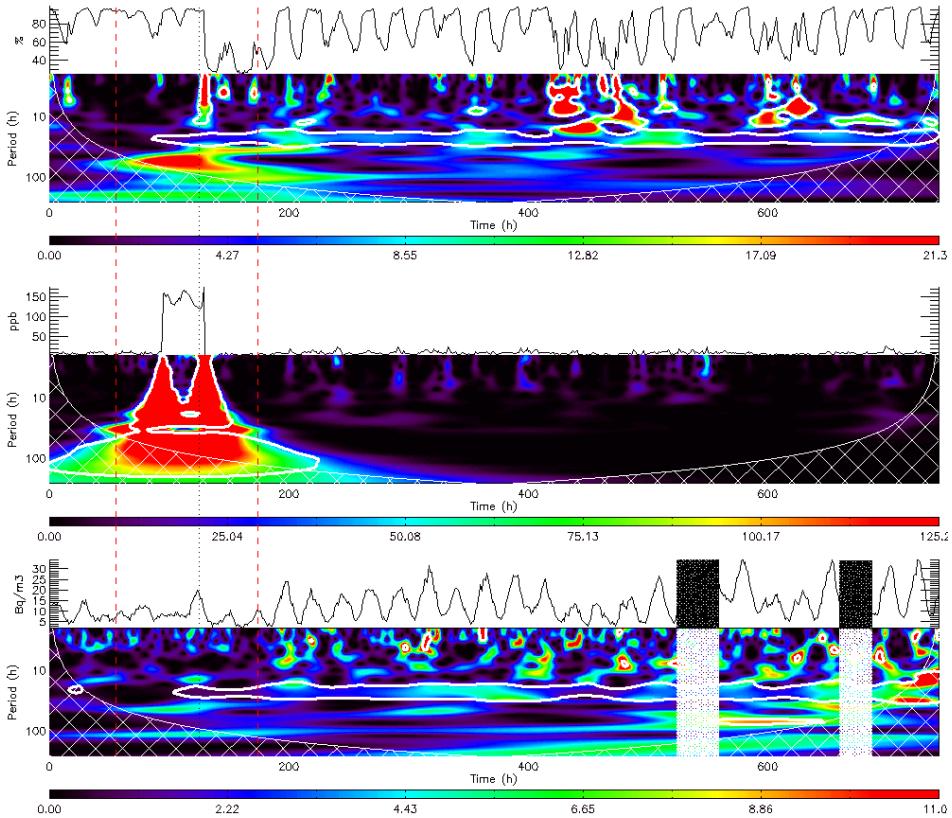

Fig. 7. Continued.

ACPD

5, 12895–12937, 2005

^{222}Rn concentration in the atmospheric surface layer

S. Galmarini

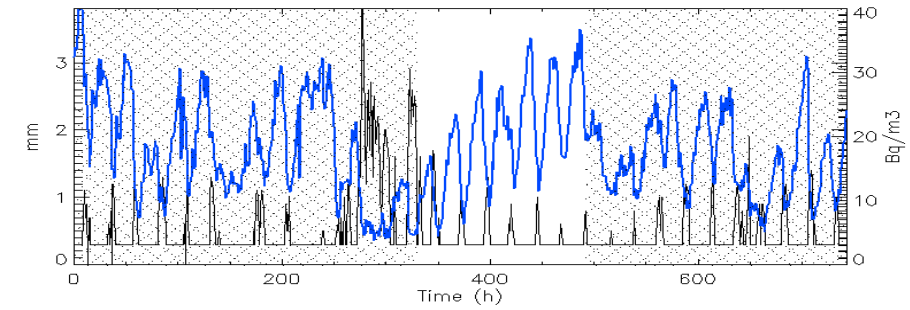

a)

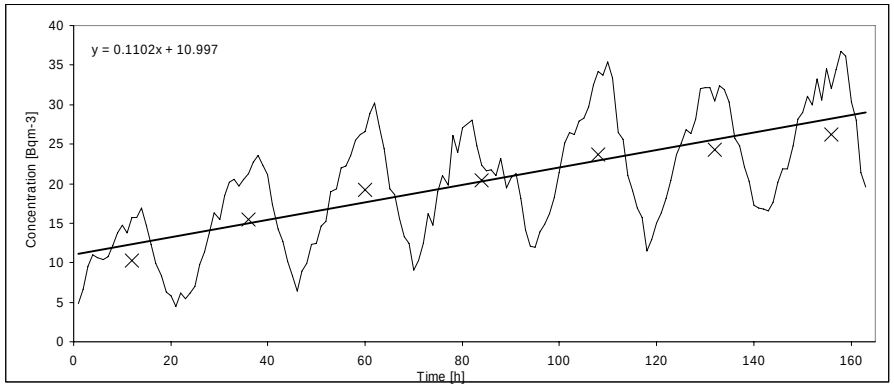

b)

Fig. 8. (a) Radon and precipitation time series during the month of October 1997. **(b)** Blow up of the time series portion of (a) not hatched. Crosses correspond to daily average values.

ACPD

5, 12895–12937, 2005

^{222}Rn concentration in the atmospheric surface layer

S. Galmarini

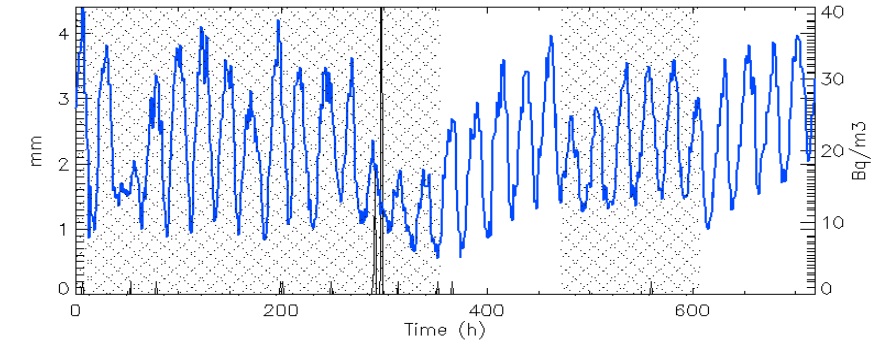

a)

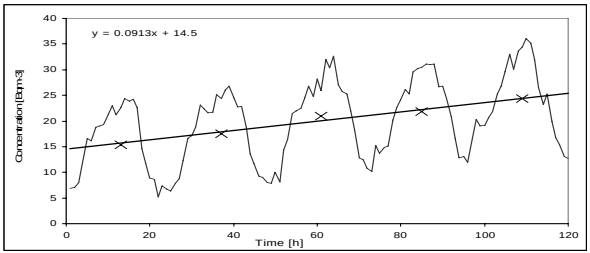

b)

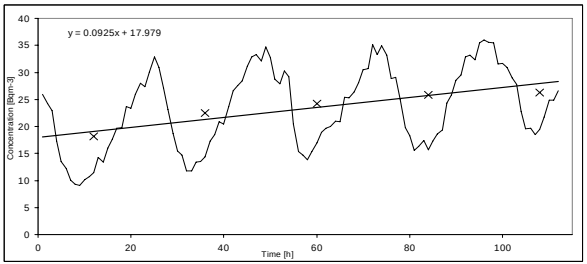

c)

Fig. 9. (a) Radon and precipitation time series during the month of September 1997. **(b)** and **(c)** Blow ups of the time series portion of (a) not hatched. Crosses correspond to daily average values.

ACPD
5, 12895–12937, 2005

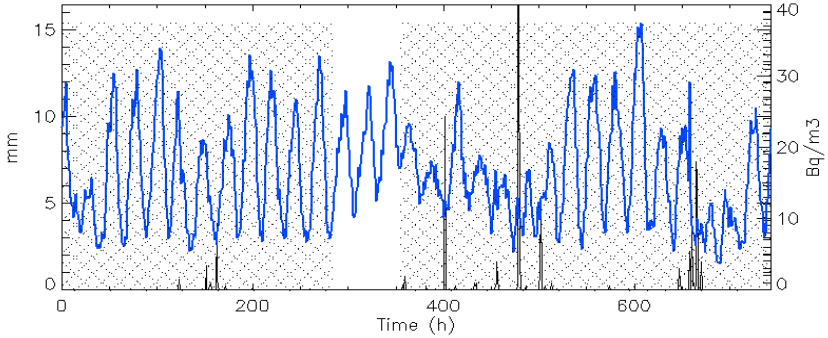

a)

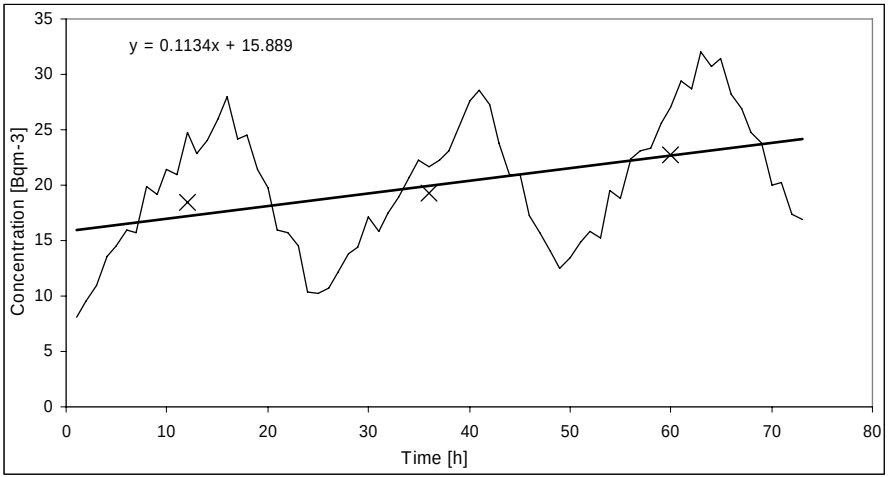

b)

Fig. 10. (a) Radon and precipitation time series during the month of August 1997. **(b)** Blow up of the time series portion of (a) not hatched. Crosses correspond to daily average values.

ACPD

5, 12895–12937, 2005

^{222}Rn concentration in the atmospheric surface layer

S. Galmarini

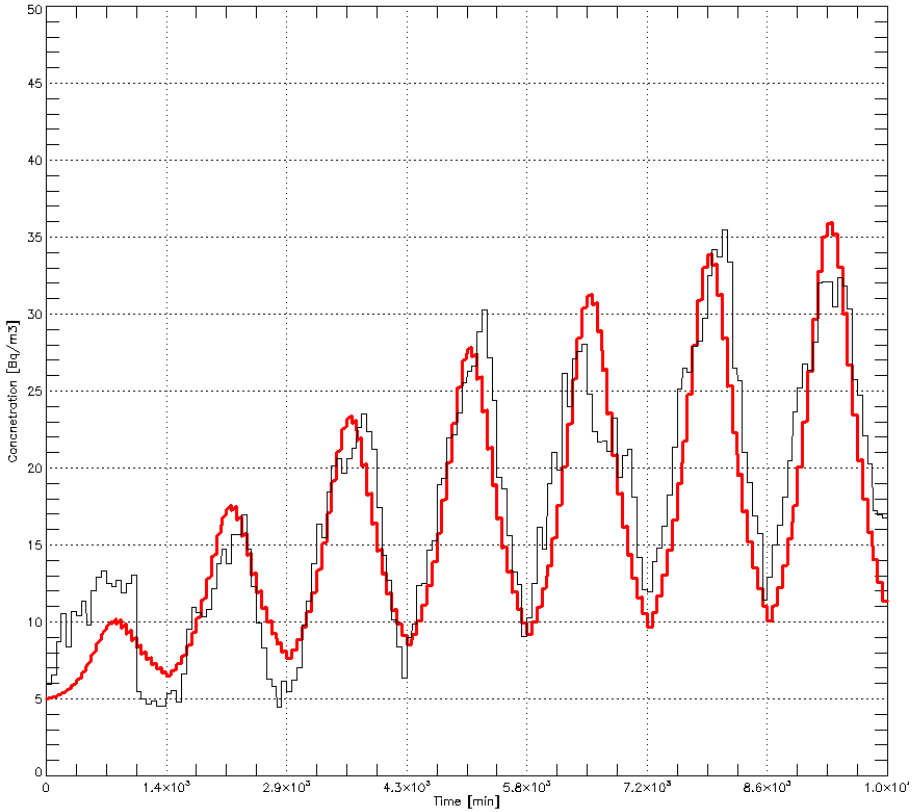

Fig. 11. Time evolution of the radon concentration presented in Fig. 8a (black curve), and modeled time series (red curve).

ACPD
5, 12895–12937, 2005

^{222}Rn concentration in the atmospheric surface layer

S. Galmarini